Article

Numerical Investigation of the Influence of a Splitter Plate on Mixing Transfer in the Ducts of a Rotary Energy Recovery Device

Kai Liu [1,2], Xuyu Liu [2], Lijuan Wu [2], Xingkai Zhang [1,2], Baocheng Shi [1,2] and Lixing Zheng [3,*]

1   Cooperative Innovation Center of Unconventional Oil and Gas, Yangtze University, Wuhan 430100, China; liukai@yangtzeu.edu.cn (K.L.); 516101@yangytzedu.com.cn (X.Z.); shibaoch@yangteu.edu.cn (B.S.)
2   Key Laboratory of Drilling and Production Engineering for Oil and Gas, Wuhan 430100, China; 519003@yangtzeu.edu.cn (X.L.); 500572@yangytzedu.com.cn (L.W.)
3   School of Electric Power, Civil Engineering and Architecture, Shanxi University, Taiyuan 030006, China
*   Correspondence: lxzheng@sxu.edu.cn

Abstract: The rotary energy recovery device (RERD) is integral in reducing energy consumption in desalination processes. The absence of a physical piston in RERD ducts allows salinity transfer from the brine to the seawater stream, which reduces RERD efficiency. To address this challenge, this study investigates the potential of utilizing splitter plates as a flow control technique to decrease the mixing degree within RERDs. Numerical simulations were performed to examine five different splitter plate configurations in RERD ducts in order to identify optimal designs for reducing the mixing degree. The analysis of internal streamlines and vortex distributions revealed that horizontal splitter plates positioned at the duct inlet effectively suppressed swirling flows, while splitter plates positioned at the center of the duct suppressed the formation of flow-induced vortices. This resulted in a more uniform salinity distribution and a reduction in the mass transfer rate between brine and seawater streams. The most significant reduction in the volumetric mixing rate was observed when employing cross-spread splitter plates positioned at the center of the duct. This paper presents an innovative method to reduce the mixing degree in the RERD.

Keywords: RO; ERD; mixing; splitter plate

1. Introduction

Water resource scarcity has become an escalating global concern due to rapid societal development. To meet the increasing demand for fresh water, seawater desalination technology has been extensively adopted worldwide and is an important technology for obtaining freshwater resources from seawater. Reverse osmosis (RO) membrane technology, considered the most advanced water purification method, efficiently removes salt and minerals from saline water [1–3]. Despite having lower operational energy requirements compared to distillation technology, RO technology still accounts for 50–70% of total operating costs in wastewater treatment [4]. This leads to higher costs for desalinated water for end-users. Consequently, energy recovery devices (ERDs), an essential part of reverse osmosis systems, are designed to maximize electricity consumption reduction. Among isobaric ERDs, rotary and piston types, both relying on the positive displacement principle, play a key role by recovering energy from high-pressure brine streams [5]. A schematic diagram of rotary-type energy recovery device (RERD) is presented in Figure 1. The RERD operates as a rotary device, efficiently recovering pressure energy from a high-pressure brine stream and transmitting it to a low-pressure seawater stream through a rotating rotor equipped with ducts. This design allows for highly effective hydraulic energy recovery. Current RERDs generally exhibit excellent energy transfer efficiency ranging from 92% to 97% [6,7]. Some advanced models, such as the iSave series from PX company, have

achieved even higher efficiencies of up to 98% [3]. This enhanced energy recovery efficiency has led to the widespread adoption of RERDs over Francis turbines in current RO plants [8].
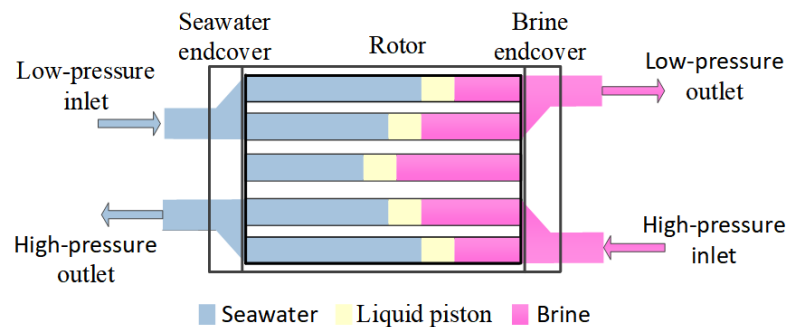

Figure 1. Schematic representation of RERD.

Notably, RERDs are distinctive due to the absence of a physical piston within their ducts, which permits a direct interaction between the two streams, as depicted in Figure 1, facilitating a high-pressure energy recovery with minimal vibration and noise levels compared to piston-type ERDs [9]. However, this approach's drawback lies in the fact that the absence of a physical piston causes salinity transfer from the brine streams back to the seawater during the work, lowering the RERD efficiency [10]. Higher seawater salinity in the RO system requires higher operating pressure from high-pressure pumps to separate salt and water, increasing energy consumption. According to the research by Cameron [11], a 2.5% increase in the salinity resulted in an approximately 1.3 bar rise in the operating pressure, which will significantly increase the energy consumption of the high-pressure pump. Therefore, it is crucial to research and develop effective methods to minimize mixing, improving long-term RERD efficiency and enhancing overall desalination plant productivity.

Techniques to reduce mixing in RERDs include over-flushing the seawater stream, adjusting operational parameters, and modifying structural design. Over-flushing involves controlling the seawater flow rate to exceed the brine flow rate, thereby pushing the high-salinity mixing zone out of the duct [12,13]. However, it requires extensive pretreatment and chemical cleaning, which increases costs. Consequently, over-flushing is not the most favorable solution for mitigating mixing degree in RERDs due to the associated high pretreatment costs [14].

Instead, recent research has focused more on optimizing operational parameters, including rotation speed and inlet flow rate, as well as structural modifications, such as duct length to control internal flows and reduce the mixing. A brief summary of key findings is presented in Table 1. These investigations have demonstrated that the adjustment of parameters, such as rotor rotation speed, inflow rate, and duct length, can influence the formation and movement of the mixing zone, also referred to as the liquid piston. However, it is essential to note that certain trade-offs exist in these approaches. For instance, increasing the rotor rotation speed can effectively reduce the mixing degree, but it comes at the cost of higher electricity consumption for the drive motor. On the other hand, decreasing the inflow rate may effectively lower the mixing degree but could also lead to reduced equipment throughput per unit of time. These trade-offs should be carefully considered when optimizing the design and operation of RERDs for specific applications. Moreover, the studies mentioned above did not examine the mechanisms by which these factors impact the mixing process from the perspective of fluid dynamics.

In our previous research [15], we conducted particle image velocimetry experiments and simulations to investigate the internal flow of RERDs. This investigation unveiled the occurrence of the "entrance effect" phenomenon at the entrance of the duct and the formation of vortices within the central region of the ducts, both of which were closely associated with the mixing process in RERDs. Furthermore, our research revealed that operational and structural parameters demonstrated a certain level of influence on the mixing degree, but they were unable to completely eliminate the "entrance effect" and the

formation of vortices within the ducts. These findings confirm that an inherent mixing zone within the RERD duct is an unavoidable outcome in the absence of a physical piston. Therefore, new methods need to be employed to suppress vortex formation, thereby inhibiting the development of the mixing zone and ultimately achieving the goal of reducing the mixing. In the research of flow control, the splitter plate has been introduced as an easier-to-implement flow control technique, requiring no additional power inputs. It has proven highly effective in suppressing vortex formation [16]. In our series of visualization experiments, we observed that splitter plates could stabilize the vortex within the near-wake region, delay the interaction between the upper and lower shear layers, and effectively alter and suppress vortex shedding in our research on flow over a bluff body [17]. This research has sparked our interest in exploring the possibility of application splitter plates into RERD studies to eliminate the "entrance effect" and suppress the formation of vortices within the ducts.

Table 1. Summary of the literature review on RERD articles.

Reference	Volumetric Mixing Rate	Method
Zhou et al. [18]	3~16%	Adjusting operational parameters
Liu et al. [19]	3~6%	Adjusting operational parameters
Xu et al. [20]	2~10%	Adjusting operational parameters
Wu et al. [21]	2~9%	Endcover with groove-textured surface
Xu et al. [22]	2~9%	Adjusting operational parameters
Yin et al. [23]	2~6%	Adjusting operational and structural parameters
Cao et al. [24]	1–4%	Endcover with extended angle

The present study aims to examine the effects of splitter plates on flow characteristics in RERDs through simulation. By investigating various configurations of splitter plates, including different placements and geometries, we seek to identify optimal splitter plate configurations for suppressing vortex formation and minimizing mixing rates in ducts. These findings can inform optimal design strategies to enhance the efficiency of RERD systems.

2. Numerical Methods

The geometric model of the RERD is shown in Figure 2. The geometric model created by the ICEM software 16.0 contains four fluid passages (a high-pressure inlet, a high-pressure outlet, a low-pressure inlet, and a low-pressure outlet), twelve rotary ducts, and two stationary end covers. The internal cross-sectional dimensions of each duct were 30 mm $\times$ 30 mm, with a length of L_0 = 265 mm.

Two critical aspects of this study will be explored: the impact of splitter plate placement on the "entrance effect" and its influence on the "liquid piston". We aimed to provide a comprehensive examination of how these placements at the duct inlet and center affect the mixing transfer within the ducts, respectively. Therefore, five different configurations, as depicted in Figure 3, were examined. The control case C0 served as the baseline with no splitter plates. To evaluate the influence on the "duct entrance", vertical and horizontal splitter plates were introduced at the duct inlet in experimental cases C1 and C2, respectively. For assessing their effect on the "liquid piston", central vertical and horizontal plates were utilized in experimental cases C3 and C4, respectively. Finally, the combined effect was explored by using both vertical and horizontal central plates in experimental case C5. In all experimental cases, the splitter plate length was $1/3\,L_0$, and thickness was 1 mm. The aim was to provide a thorough analysis of the outcomes and implications of these configurations for a deeper understanding of their effects on the mixing degree.
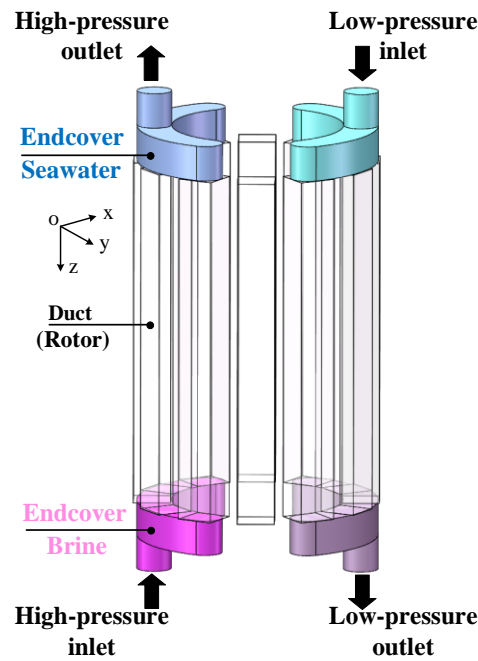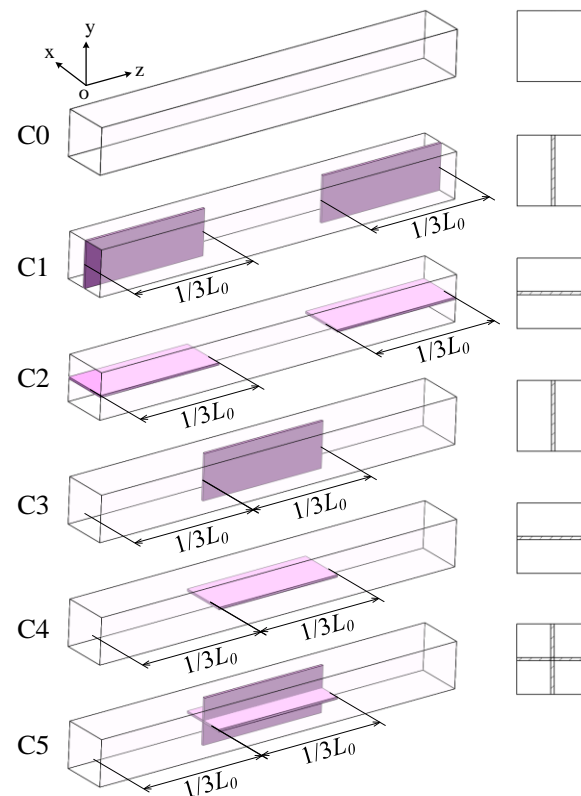
Figure 2. Geometric model.

Figure 3. Illustrations of five different splitter plate configurations.

Fluid domain spatial discretization and structured hexahedral meshing were performed in ICEM software 16.0, generating approximately 800 k computational cells. For the unsteady and incompressible calculations, Ansys Fluent 16.0 was utilized. Heat transfer was ignored due to minimal temperature differences between the streams. To accurately capture strong unsteadiness and uncover mixing motions and flow fields in the ducts during the RERD operation, the realizable *k-ε* (RKE) turbulence model was employed as it provided improved accuracy for high unsteadiness based on our previous research [15].

The CFD model employed a pressure-based solver. To discretize the convective terms, a second-order upwind scheme was implemented. A second-order upwind scheme discretized the convective terms of each equation. The time step was 1×10^{-3} s, with a convergence criterion of 1×10^{-4}. The total timestep number was 1×10^{5}, equivalent to 20 RERD rotations.

The turbulent mixing process in flows can be calculated using the species transport equation, shown as:

$$\frac{\partial}{\partial t}(\rho Y_{i}) + \nabla \cdot (\rho \vec{u} Y_{i}) = -\nabla \cdot \vec{J}_{i} \tag{1}$$

Here, Y_{i} represents the mass fraction of species *i*, and $\vec{J}_{i}$ denotes the diffusion flux, defined as:

$$\vec{J}_{i} = -\left(\frac{\mu_{t}}{Sc_{t}} + \rho D_{i,m} \right) \tag{2}$$

where $D_{i,m}$ denotes the mass diffusion coefficient, Sc_{t} is the turbulent Schmidt number, and μ_{t} represents the turbulent viscosity.

Velocity boundary conditions were employed for the high-pressure inlet and low-pressure inlet, with the corresponding inflow rate set at 3.6 m^3/h. Pressure boundary conditions were employed for the high-pressure outlet and low-pressure outlet, and the corresponding pressure was set as 6.0 MPa and 0.2 MPa, respectively. The desalination process in calculations was simulated using 3.5 g/L NaCl solutions for brine and 1.8 g/L NaCl solutions for seawater streams. The other walls of the RERD were assigned the velocity no-slip wall boundary condition. A sliding mesh method was utilized to simulate the relative rotational motion between the ducts and endcover. The contact surfaces of the two parts were defined as interfaces for data transmission during the calculations. The duct rotational speed was 120 rpm. Our previous CFD simulations and PIV experiments demonstrated good agreement, validating the computational approach [15].

3. Results

3.1. Results of Volumetric Mixing Rate

To quantify mixing between the brine and seawater streams, a volumetric mixing rate M_{x} was defined as:

$$M_{x} = (C_{\text{HP-out}} - C_{\text{LP-in}})/(C_{\text{HP-in}} - C_{\text{LP-in}}) \tag{3}$$

where $C_{\text{HP-out}}$ was the salinity concentration at the high-pressure outlet, $C_{\text{LP-in}}$ was the concentration at the low-pressure inlet, and $C_{\text{HP-in}}$ was the inlet concentration of the HP stream.

Figure 4 presents the influence of splitter plates on the volumetric mixing rate. In comparing these results to those from previous studies presented in Table 1, the volumetric mixing rate for the control case C0 fell within a reasonable range. However, it becomes evident that the utilization of splitter plates led to a reduction in the volumetric mixing rate across all experimental cases. Moreover, it is important to highlight that the effect of splitter plates on the volumetric mixing degree varied significantly depending on their specific structural arrangements. When the splitter plates were positioned at the duct's inlet, the experimental case C2 with transverse splitter plates demonstrated a lower volumetric mixing rate when compared to the experimental case C1 with longitudinal splitter plates. Conversely, when the splitter plates were placed at the center of the duct, both the experimental cases C4 and C5 with transverse and cross-spread splitter plates, respectively, exhibited superior performance in controlling the mixing transfer process. Notably, the C5 case recorded a remarkable 57% reduction in volumetric mixing rate compared to the control case C0, highlighting that the utilization of cross-spread splitter plates in the C5 case proved to be the most effective in suppressing the volumetric mixing rate.
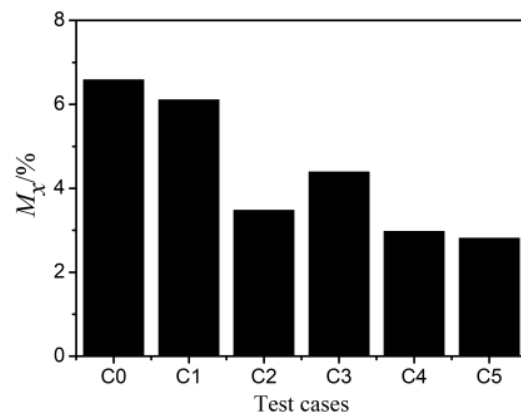
Figure 4. Variation of volumetric mixing rate with various splitter plate configurations.

In summary, those results demonstrate that placing the splitter plates at the center of the duct yields superior effectiveness in controlling the volumetric mixing rate compared to placing them at the duct inlet. To gain a comprehensive understanding of how splitter plates influence the volumetric mixing rate of the device, it is essential to conduct thorough research on flow distribution and mixing motion in the ducts.

3.2. The Control Effect of Splitter Plates on the "Entrance Effect"

For the convenience of describing the flow process in ducts, the working process of the RERD was divided into 12 working phases during one complete rotation, as illustrated in Figure 5. Among these phases, four specific phases in the sealed stage and the seawater supercharging stage had been selected for research.
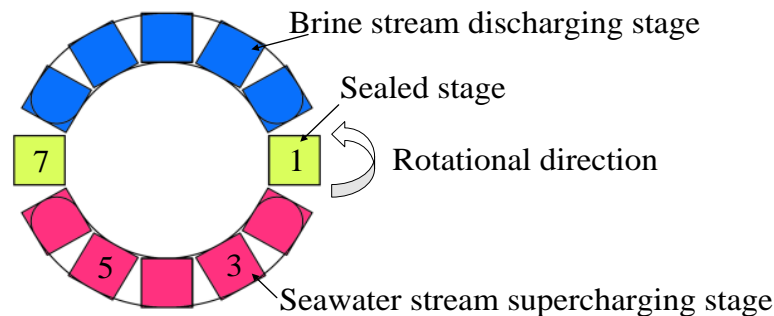

Figure 5. Twelve working phases during one complete rotation.

Figure 6 illustrates the streamline distributions in the ducts for cases C0, C1, and C2. It was observed that the flow structures in the experimental case C1 closely resembled that of the control case C0, with the size of the swirling flow region at the duct inlet remaining largely unchanged. However, in the experimental case C2, a significant impact on the flow distributions at the left and right sides of the duct was observed. The presence of the splitter plate in the experimental case C2 effectively suppressed the swirling flow at the duct inlet, splitting it into two smaller swirling flows—one above and the other below the splitter plate. The size of these swirling flows was notably reduced in the downstream direction. Nevertheless, it is important to note that the streamlines in the center region of the duct for experimental cases C1 and C2 were approximately similar to those in the control case C0. These findings indicated that the arrangement of splitter plates for experimental cases C1 and C2 had a minimal effect on the flow process in the center region of ducts.
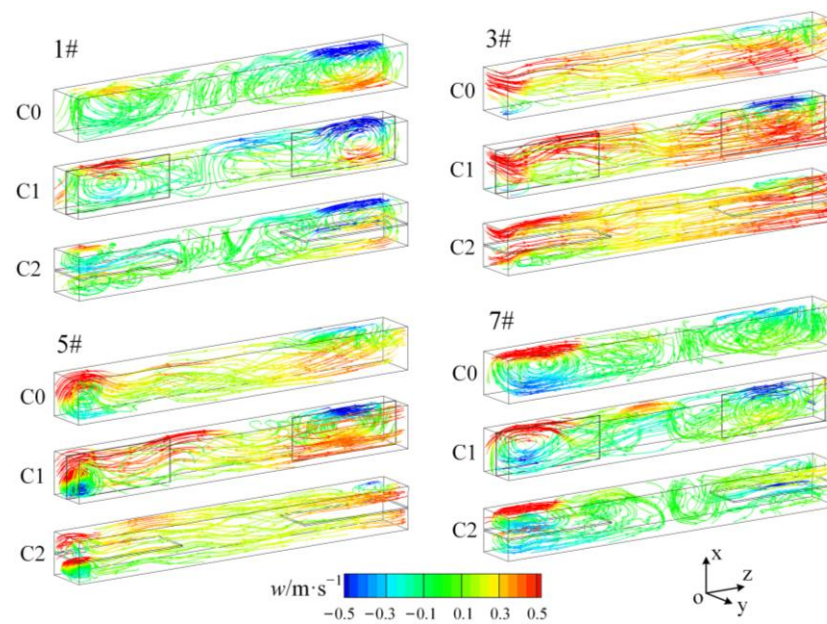
Figure 6. Streamline plots showing the control effect of splitter plates on the "entrance effect".

To give a more thorough understanding of the control influence of the splitter plate on the internal mixing and reveal the complex flow structures, the Q criterion [25] was proposed to identify the vortex structures in the internal flow structures. Figure 7 illustrates the influence of splitter plates on the formation and evolution of vortices for cases C0, C1, and C2. The splitter plates in these experimental cases exhibited a significant control effect on the "entrance effect". In the experimental case C1, the vortices at the duct inlet were longitudinally divided into two parts, with the vortex structure on the left side of the splitter plate being notably larger than the one on the right side. However, the influence of the splitter plate on the size of the vortices at the duct inlet in the downstream direction was quite limited. The streamwise dimension of the vortices in the experimental case C1 was similar to that of the control case C0. Compared to the results of the experimental case C1, the splitter plate in the experimental case C2 significantly suppressed the vortex structures at the duct inlet, effectively controlling fluid instability in this region. This observation provided an explanation for the smaller volumetric mixing degree of experimental case C2 compared to experimental case C1 in Figure 4.

In phase 5#, a separation vortex structure, indicated by the orange arrow, was observed at the end of the splitter plate in the experimental case C1. This separation vortex structure could increase fluid instability, leading to a higher mass transfer rate in the center of the duct. According to previous research [26,27], the interface between the seawater and brine streams was located in the central region of the duct, known as the mixing zone. Increasing the mass transfer rate in the mixing zone would result in the transfer of salt from the brine stream to the seawater stream, eventually leading to a higher volumetric mixing rate of the device. The implementation of longitudinal splitter plates in the experimental case C1 suppressed the "entrance effect", but it also led to increased fluid instability in the mixing zone. As a result, the longitudinal splitter plate in the experimental case C1 had a weaker effect on reducing the volume mixing rate of the device, as shown in Figure 4. On the other hand, the experimental case C2, with a transverse splitter plate, not only effectively suppressed the "entrance effect" but also avoided an increase in fluid instability in the mixing zone. Consequently, experimental case C2 could achieve a relatively lower volume mixing rate, as depicted in Figure 4.
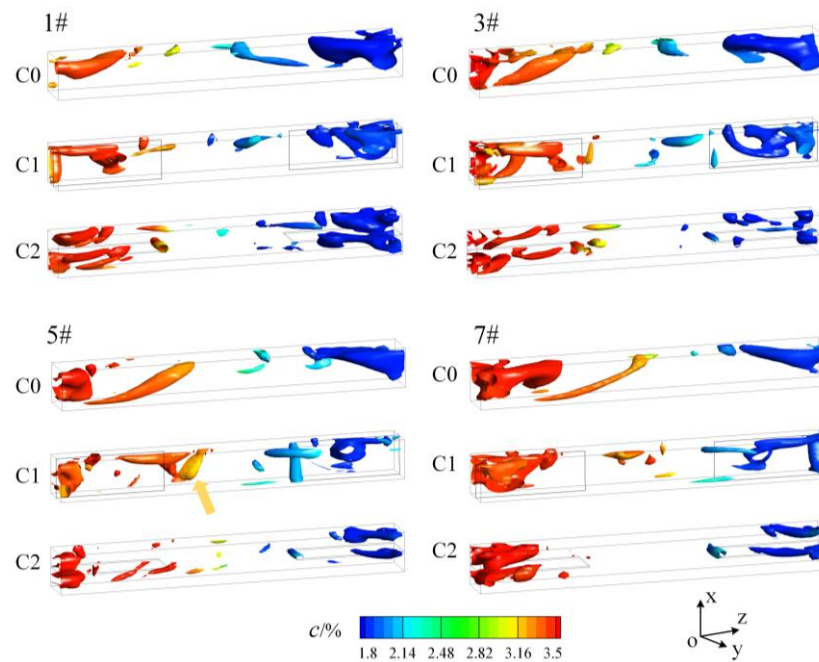
Figure 7. *Q* criterion iso-surface (*Q* = 0.02) colored by salinity magnitude for cases of C0, C1, and C2. Orange arrow indicates a separation vortex structure.

Figure 8 illustrates the relationship between the salinity distribution and working phases. In phase 1#, the control case C0 exhibited a clear high-concentration mixing region on the right side of the duct, as indicated by the red arrow, the location of which corresponded to the vortex shown in Figure 7. As the brine stream flowed into the duct, this high-concentration mixing region was pushed forward, leading to the transfer of salt to the seawater stream. Consequently, there was a significant increase in salt concentration on the right side of the duct in phase 3#. As a result, the discharged seawater contained a high salt concentration, contributing to the increase in the volume mixing rate of the device.
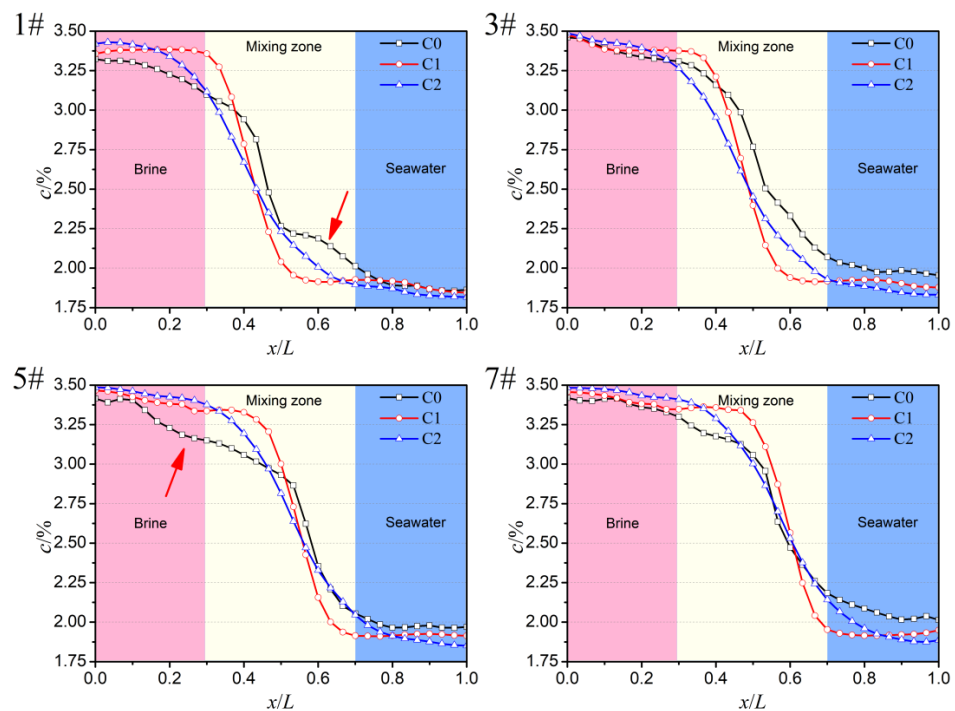

Figure 8. Salinity distribution for cases of C0, C1, and C2. Red arrow indicates a clear high-concentration mixing region.

In phase 5 of the control case C0, a low-concentration mixing region formed on the left side of the duct, as indicated by the red arrow, corresponding to the vortex shown in Figure 7. The presence of splitter plates in the experimental cases C1 and C2 had a controlling effect on the vortices, leading to weakened vortex structures and reduced flow intensity compared to those in the control case C0, as evident from Figure 7. As a result, there were no high- or low-concentration mixing regions in both phases 1# and 5#, as shown in Figure 8. Furthermore, the salt concentration distribution on both sides of the duct in the experimental case C2 case was more uniform, indicating that the experimental case C2 with a transverse splitter plate arrangement had a more effective control effect on the mixing process in the ducts.

3.3. The Control Effect of Splitter Plates on the Liquid Piston

Figure 9 displays the streamline distributions in the ducts for the cases of C0, C3, C4, and C5. Comparing the streamlines with those of the control case C0, it can be observed that the splitter plates in experimental cases C3, C4, and C5 had a limited impact on the "entrance effect". However, they exhibited significant control on the flow field in the center of the duct. From the streamline distributions, it can be observed in the sealed stages (phase 1# and 7#), the center region of the ducts in the control case C0 exhibited significant mixing flow. In contrast, the presence of splitter plates in the experimental cases C4 and C5 suppressed the mixing flow in that region, causing the fluid to flow only within the small chambers isolated by the splitter plates. Furthermore, under the influence of the Coriolis force [28], swirling flow was observed in the center of the ducts in the control case C0. However, due to the presence of the splitter plates in experimental cases C4 and C5, the swirling flow was confined within each small chamber, preventing mass transfer between different streams. This phenomenon contributed to a reduction in the mixing rate between the brine and seawater streams.
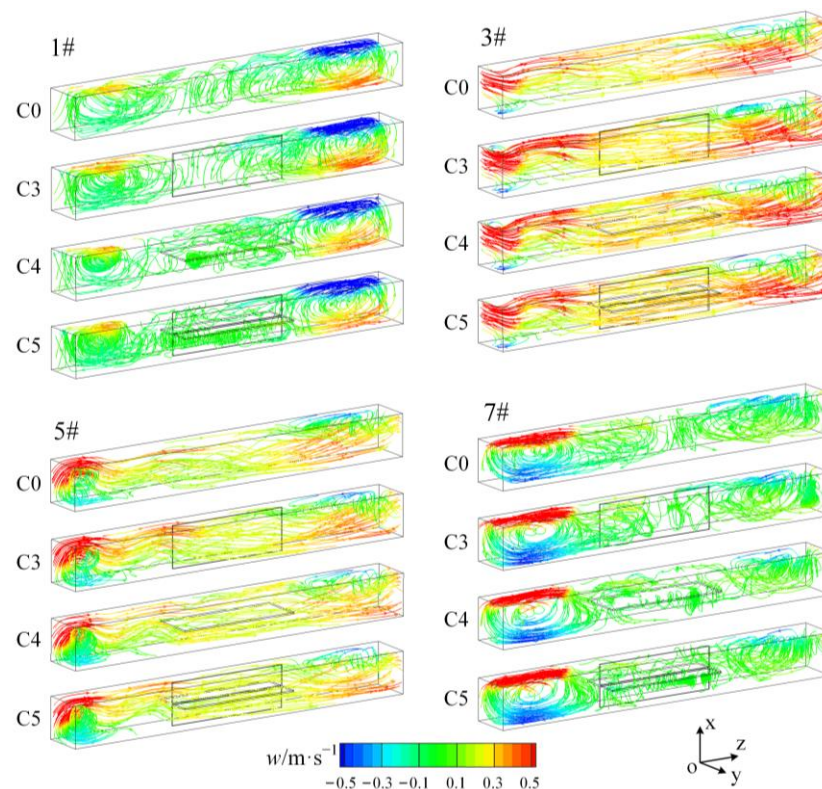

Figure 9. Streamline plots showing the control effect of splitter plates on the liquid piston.

Figure 10 illustrates the influence of splitter plates on the formation and evolution of vortices for the cases of C0, C3, C4, and C5. The results indicate that the vortices at the left and right sides of the ducts were hardly affected by the splitter plates, confirming that these splitter plate configurations for experimental cases C3, C4, and C5 had no suppressive effect on the "entrance effect". In the center of the ducts, the vortices induced by the Coriolis force, as indicated by the green arrows, were clearly observed in experimental cases C4 and C5. However, in phase 7# of experimental cases C4 and C5, the size of the separation vortices induced by the "entrance effect" [15] significantly decreased, demonstrating that the suppressive effect of the splitter plates was most pronounced at this stage. This indicated that the positioning and structure of the splitter plates in the experimental cases C4 and C5 were especially effective in controlling vortex formation and fluid instability in the ducts.
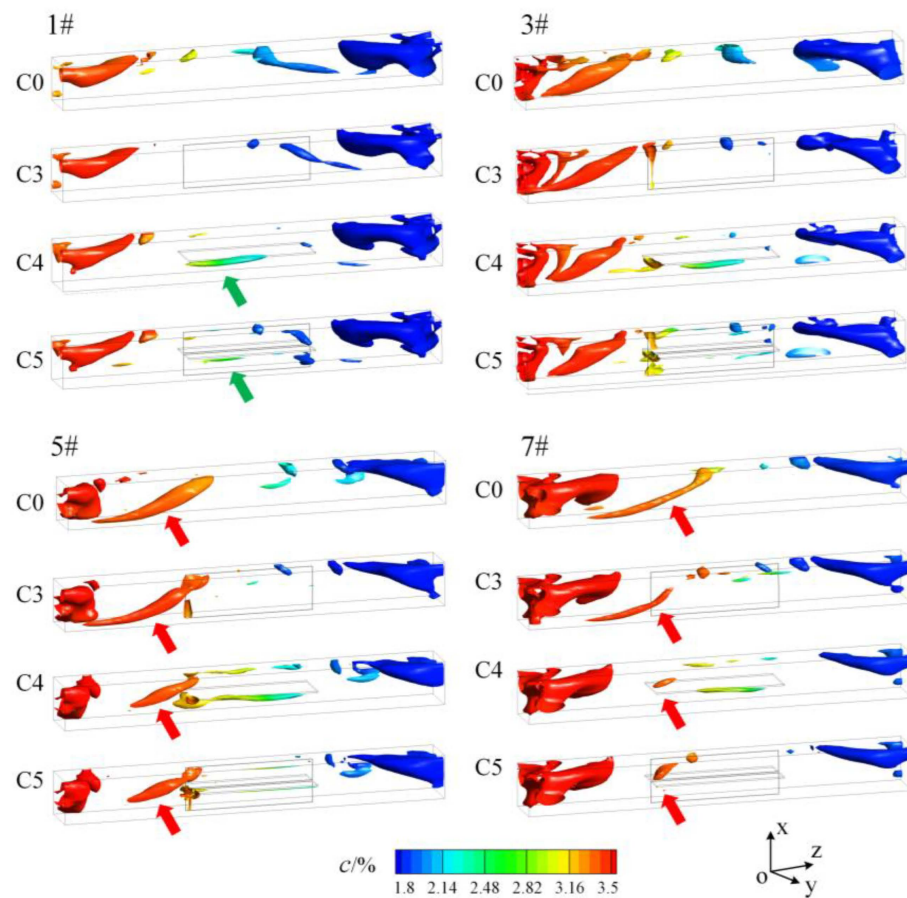

Figure 10. *Q* criterion iso-surface (*Q* = 0.02) colored by salinity magnitude for cases of C0, C3, C4, and C5. Green arrow indicates vortices induced by the Coriolis force. The red arrow indicates the "entrance effect" phenomenon, which is the vortex formed at the duct entrance.

Figure 11 illustrates the relationship between the salinity distribution and working phases for the cases of C0, C3, C4, and C5. Due to the efficient suppression of flow instabilities in the ducts by the splitter plates in experimental cases C4 and C5, no high- or low-concentration mixing regions were observed in any phases. Combining these results with those from Figure 10, it can be inferred that if the separation vortices induced by the "entrance effect" can be effectively suppressed and prevented from entering the center of the ducts, the splitter plate, as a passive control technique, can effectively reduce the mass transfer rate between the two streams. This approach may lead to lower mixing levels and improve the pressure recovery efficiency of the RERD.
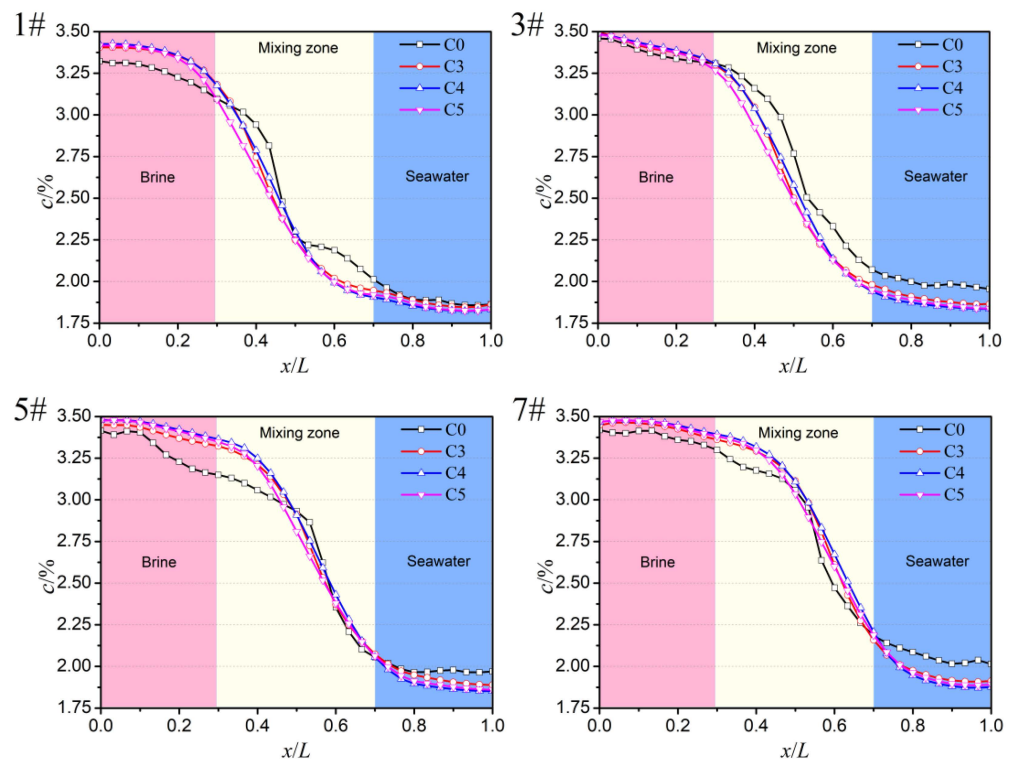
Figure 11. Salinity distribution for cases of C0, C3, C4, and C5.

4. Conclusions

In this study, we utilized numerical simulations to investigate the utilization of splitter plates in regulating the flow dynamics within RERD ducts. Our investigation, consisting of five distinct splitter plate configurations, yielded several critical conclusions regarding their impact on flow distribution and mixing dynamics:

(1) Flow structure and vortex formation control: Effective suppression of swirling flows at the entrance was achieved when horizontal splitter plates were positioned at the duct inlet (as seen in experimental case C2). Moreover, the control of flow-induced vortices generated by the "entrance effect" was efficiently executed by splitter plates positioned at the center of the duct (as seen in experimental cases C4 and C5), preventing their propagation into the central duct region.

(2) Salinity distribution and mass transfer: By efficiently suppressing the 'entrance effect' and flow-induced vortices, as observed in experimental case C2 and experimental cases C4 and C5, respectively, these configurations resulted in decreased flow intensity and the establishment of a more uniform salinity distribution. Consequently, the mass transfer between brine and seawater streams was significantly minimized.

(3) Effect of splitter plates on volumetric mixing rate: The utilization of splitter plates consistently reduced the volumetric mixing rate across all experimental cases compared to the control case. This reduction was most notable when utilizing cross-spread splitter plates positioned at the center of the duct, as evidenced in experimental case C5, where a remarkable 57% decrease in volumetric mixing rate was achieved compared to the control case.

These insights into the application and configuration of splitter plates offer valuable guidance for designing more efficient RERDs. Future work could optimize splitter plate parameters, such as shape, dimensions, spacing, alignment, and materials, to identify designs that maximally suppress mixing. Investigating the real-world applicability and scalability of effective configurations in full-scale desalination plants will be key for driving further advancements.

References

1. Tawalbeh, M.; Qalyoubi, L.; Al-Othman, A.; Qasim, M.; Shirazi, M. Insights on the development of enhanced antifouling reverse osmosis membranes: Industrial applications and challenges. *Desalination* **2023**, *553*, 116460. [CrossRef]
2. Zinatloo-Ajabshir, S.; Morassaei, M.S.; Salavati-Niasari, M. Eco-friendly synthesis of Nd2Sn2O7–based nanostructure materials using grape juice as green fuel as photocatalyst for the degradation of erythrosine. *Compos. Part B Eng.* **2019**, *167*, 643–653. [CrossRef]
3. Esfahani, M.H.; Zinatloo-Ajabshir, S.; Naji, H.; Marjerrison, C.A.; Greedan, J.E.; Behzad, M. Structural characterization, phase analysis and electrochemical hydrogen storage studies on new pyrochlore SmRETi2O7 (RE = Dy, Ho, and Yb) microstructures. *Ceram. Int.* **2023**, *49*, 253–263. [CrossRef]
4. Caldera, U.; Breyer, C. Afforesting arid land with renewable electricity and desalination to mitigate climate change. *Nat. Sustain.* **2023**, *6*, 526–538. [CrossRef]
5. Kadaj, E.; Bosleman, R. Chapter 11—Energy Recovery Devices in Membrane Desalination Processes. In *Renewable Energy Powered Desalination Handbook*; Gude, V.G., Ed.; Butterworth-Heinemann: Oxford, UK, 2018; pp. 415–444.
6. Ayaz, M.; Namazi, M.A.; Din, M.A.; Ershath, M.I.M.; Mansour, A.; Aggoune, e.-H.M. Sustainable seawater desalination: Current status, environmental implications and future expectations. *Desalination* **2022**, *540*, 116022. [CrossRef]
7. Nassrullah, H.; Anis, S.F.; Hashaikeh, R.; Hilal, N. Energy for desalination: A state-of-the-art review. *Desalination* **2020**, *491*, 114569. [CrossRef]
8. Wang, C.; Meng, P.; Wang, S.; Song, D.; Xiao, Y.; Zhang, Y.; Ma, Q.; Liu, S.; Wang, K.; Zhang, Y. Comparison of two types of energy recovery devices: Pressure exchanger and turbine in an island desalination project case. *Desalination* **2022**, *533*, 115752. [CrossRef]
9. Stover, R.L. Seawater reverse osmosis with isobaric energy recovery devices. *Desalination* **2007**, *203*, 168–175. [CrossRef]
10. Bross, S.; Kochanowski, W. SWRO core hydraulic system: Extension of the SalTec DT to higher flows and lower energy consumption. *Desalination* **2007**, *203*, 160–167. [CrossRef]
11. Cameron, I.B.; Clemente, R.B. SWRO with ERI's PX Pressure Exchanger device—A global survey. *Desalination* **2008**, *221*, 136–142. [CrossRef]
12. Stover, R.; Fernandez, A.O.; Galtes, J. Permeate Recovery Rate Optimization at the Alicante Spain SWRO Plant. In Proceedings of the International Desalination Association World Congress, Dubai, United Arab Emirates, 7–12 November 2009.
13. Schneider, B. Desalination and the Environment Selection, operation and control of a work exchanger energy recovery system based on the Singapore project. *Desalination* **2005**, *184*, 197–210. [CrossRef]
14. Goto, A.; Shinoda, M.; Takemura, T. Mixing Control in an Isobaric Energy Recovery Device of Seawater Reverse Osmosis Desalination System. In *ASME 2017 Fluids Engineering Division Summer Meeting*; American Society of Mechanical Engineers: New York, NY, USA, 2017; p. V01BT08A003.
15. Liu, K.; Deng, J.; Ye, F. Numerical simulation of flow structures in a rotary type energy recovery device. *Desalination* **2019**, *449*, 101–110. [CrossRef]
16. Zhao, M. A review of recent studies on the control of vortex-induced vibration of circular cylinders. *Ocean Eng.* **2023**, *285*, 115389. [CrossRef]
17. Islam, S.; Rahman, H.; Abbasi, W.; Noreen, U.; Khan, A. Suppression of fluid force on flow past a square cylinder with a detached flat plate at low Reynolds number for various spacing ratios. *J. Mech. Sci. Technol.* **2014**, *28*, 4969–4978. [CrossRef]

18. Zhou, Y.H.; Ding, X.W.; Ju, M.W.; Chang, Y.Q. Numerical simulation on a dynamic mixing process in ducts of a rotary pressure exchanger for SWRO. *Desalin. Water Treat.* **2009**, *1*, 107–113. [CrossRef]

19. Liu, Y.; Zhou, Y.; Bi, M. 3D numerical simulation on mixing process in ducts of rotary pressure exchanger. *Desalin. Water Treat.* **2012**, *42*, 269–273.

20. Xu, E.L.; Wang, Y.; Wu, L.M.; Xu, S.C.; Wang, Y.X.; Wang, S.C. Computational fluid dynamics simulation of brine-seawater mixing in a rotary energy recovery device. *Ind. Eng. Chem. Res.* **2014**, *53*, 18304–18310. [CrossRef]

21. Wu, L.M.; Wang, Y.; Xu, E.L.; Wu, J.N.; Xu, S.C. Employing groove-textured surface to improve operational performance of rotary energy recovery device in membrane desalination system. *Desalination* **2015**, *369*, 91–96. [CrossRef]

22. Xu, E.L.; Jianga, X.; Miaoa, Z.; Wangc, F. Comparing brine-seawater mixing between two-port and four-port rotary energy recovery device. *Desalin. Water Treat.* **2020**, *173*, 207–212. [CrossRef]

23. Yin, F.L.; Nie, S.L.; Ji, H.; Lou, F.L. Numerical study of structure parameters on energy transfer and flow characteristics of integrated energy recovery and pressure boost device. *Desalin. Water Treat.* **2018**, *131*, 141–154. [CrossRef]

24. Cao, Z.; Deng, J.; Yuan, W.; Chen, Z. Integration of CFD and RTD analysis in flow pattern and mixing behavior of rotary pressure exchanger with extended angle. *Desalin. Water Treat.* **2015**, *57*, 15265–15275. [CrossRef]

25. Liu, Y.; Zhong, W.; Tang, Y. On the relationships between different vortex identification methods based on local trace criterion. *Phys. Fluids* **2021**, *33*, 105116. [CrossRef]

26. Yin, F.; Nie, S.; Hou, W.; Xiao, S. Effect analysis of silencing grooves on pressure and vibration characteristics of seawater axial piston pump. *Proc. Inst. Mech.Eng. Part C J. Mech. Eng.Sci.* **2017**, *231*, 1390–1409. [CrossRef]

27. Lou, F.; Nie, S.; Yin, F.; Lu, W.; Ji, H.; Ma, Z.; Kong, X. Numerical and experimental research on the integrated energy recovery and pressure boost device for seawater reverse os-mosis desalination system. *Desalination* **2022**, *523*, 115408. [CrossRef]

28. Liu, K.; Zheng, L. Simulation Investigation on the Flow and Mixing in Ducts of the Rotary Energy Recovery Device. *Geofluids* **2020**, *2020*, 8822493.